

# We are IntechOpen, the world's leading publisher of Open Access books Built by scientists, for scientists

6,900

Open access books available

186,000

International authors and editors

200M

Downloads

Our authors are among the

154

Countries delivered to

TOP 1%

most cited scientists

12.2%

Contributors from top 500 universities



WEB OF SCIENCE™

Selection of our books indexed in the Book Citation Index  
in Web of Science™ Core Collection (BKCI)

Interested in publishing with us?  
Contact [book.department@intechopen.com](mailto:book.department@intechopen.com)

Numbers displayed above are based on latest data collected.  
For more information visit [www.intechopen.com](http://www.intechopen.com)



---

# Femtosecond Laser-Induced Surface Modification and its Application

---

Kenji Goya, Masahiko Shiraishi, Yusuke Fuchiwaki,  
Kazuhiro Watanabe and Toshihiko Ooie

Additional information is available at the end of the chapter

<http://dx.doi.org/10.5772/65428>

---

## Abstract

In this chapter, we present femtosecond laser micromachining to fiber optics, focusing on surface qualities. Some techniques applied in the field are introduced to date and a review of some of the current applications for this type of technology. Section 2 describes laser-induced periodic surface structures (LIPSSs), which are induced in low- and high-fluence regime. Section 3 describes the influences of laser-induced structures for the fabrication of fiber-optic sensors, with experimental techniques and results in our research group. These sections explore ultrashort laser pulses applications, roughly going from lower to higher energy (power, intensity) ones.

**Keywords:** LIPSS, formation mechanism, femtosecond laser microfabrication, high-fluence regime, fiber-optic sensor

---

## 1. Introduction

Ultrashort pulse laser interaction has been attractively applied to the modification of material properties [1–8] in various materials. The ultrashort pulse laser applications to micromachining [9–16] have received much attention. This is mainly because of two reasons that are extremely high-peak power and ultrashort pulse less than material thermal relaxation. In the high-peak laser regime, multiphoton absorption can be easily induced even in transparent materials. Furthermore, the effects of thermal diffusion during material processing can be extremely minimized with ultrashort pulses that produce a thermal non-equilibrium state between electrons and lattice. Owing to such non-thermal and spatially localized effects can facilitate to

---

locate a specified volume ablation without collateral thermal damage, and microdevices can be precisely machined using femtosecond processing to produce high functionality even in a microscale platform such as thin optical fibers [17–25] or analytical microchip for biochemical application. For this reason, such processing for functional microstructures has been previously reported in the past decade.

Using femtosecond laser micromachining for such optical devices, surface characteristics should be carefully checked because the optical/mechanical properties on the laser-induced surface structures provide completely different response with dependence on micro/nanoscale conditions which is varied with laser irradiation parameters. Such surface responses can be used for controlling phenomena like wettability, reflectivity, and friction as well as biomimetics [26]. This is the reason why nanotechnology has attracted wide interest in many fields.

In this chapter, we present femtosecond laser micromachining to microdevice such as fiber optics with a focus on surface qualities. Section 2 is dedicated to laser-induced periodic surface structures (LIPSSs), which are induced in low- and high-fluence regime. The influences of laser-induced structures for the fabrication of fiber-optic sensors are described in Section 3, with experimental techniques and results in our research group. Conclusions are presented in Section 4.

## **2. Femtosecond laser-induced surface structures**

Laser-induced surface structures have been widely investigated in various materials such as metals, ceramics, glass, and polymers. A periodicity of about the wavelength  $\lambda$  of the laser radiation is commonly observed, which are usually called as ripples or laser-induced periodic surface structures (LIPSS). It should be noted that such LIPSS show water-repellent properties [12, 27–29], diffusive reflection [30–34], and friction change [35–38]. The spatial periodicity of low-spatial frequency LIPSS (LSFL) is known to be approximately laser wavelength dependent, and the LSFL is mainly orientated perpendicular to the direction of the laser polarization. LSFL and high-spatial frequency LIPSS (HSFL) generated by femtosecond laser pulses have been recently observed. Using high-energy laser pulses, micrometer-size-rugged surfaces are formed inside the channel structures ablated by femtosecond laser pulses [39–41]. It is also important to understand the formation mechanism of micrometer-scale surfaces for femtosecond laser direct writing technologies in which relatively higher laser energies are used to fabricate a 3D structure such as fluidic channels [3, 42, 43], sampling cells [19, 21, 22], and interferometers [44–46]. Different generating processes will induce different mechanical responses, which will be detailed in the following.

### **2.1. Laser-induced periodic surface structures (LIPSS)**

In 1965, LIPSS formation induced by exposing semiconductors to a ruby laser was first observed by [47]. Although LIPSS had been unfavorable as irregular structures inevitably accompanied by laser processing, the development of ultrashort pulse laser allows us to achieve not only stable periodic structures, but also non-conventional advantages based on

nanotechnologies mentioned above. Applications of LIPSS for mechanical engineering such as water-repellent property, strain relief [48], and friction control have been reported as well as for biomedical applications such as cell adhesion and its growth [49, 50]. For the case of optics, LIPSS are applied to structural coloring [51], surface-enhanced Raman spectroscopy (SERS) [52], and anti-reflection surface. Mechanism of LIPSS formation has been discussed in many literatures. Sipe et al. established a first principle for LIPSS formation process, by considering a surface-scattered wave from the surface roughness and modeling the effect of the roughness on the electromagnetic field [53–55]. **Figure 1** shows a simple model for the formation of LIPSS, showing geometry of a laser beam idealized as a finite plane wave onto a rough surface. While LSFL can be obtained by either a CW (continuous wave) laser or a pulsed laser irradiation, HSFL can only be observed for the case of using pulse laser in the duration of picosecond or femtosecond range. For linearly polarized light at a normal direction to the plane, an LIPSS periodicity becomes much smaller than the laser wavelength and their direction can be parallel [56] or orthogonal [57] to the polarization, depending on the material properties and the irradiation parameters. The nature of HSFL is still under controversially discussion, and many theories have been proposed to explain the formation mechanism: surface-plasmon polaritons [58–60], second harmonic generation [57, 61], self-organization [62–67], waveguides modes [68], parametric process [69, 70], or interference along with a modification of the optical properties during the pulse [56].

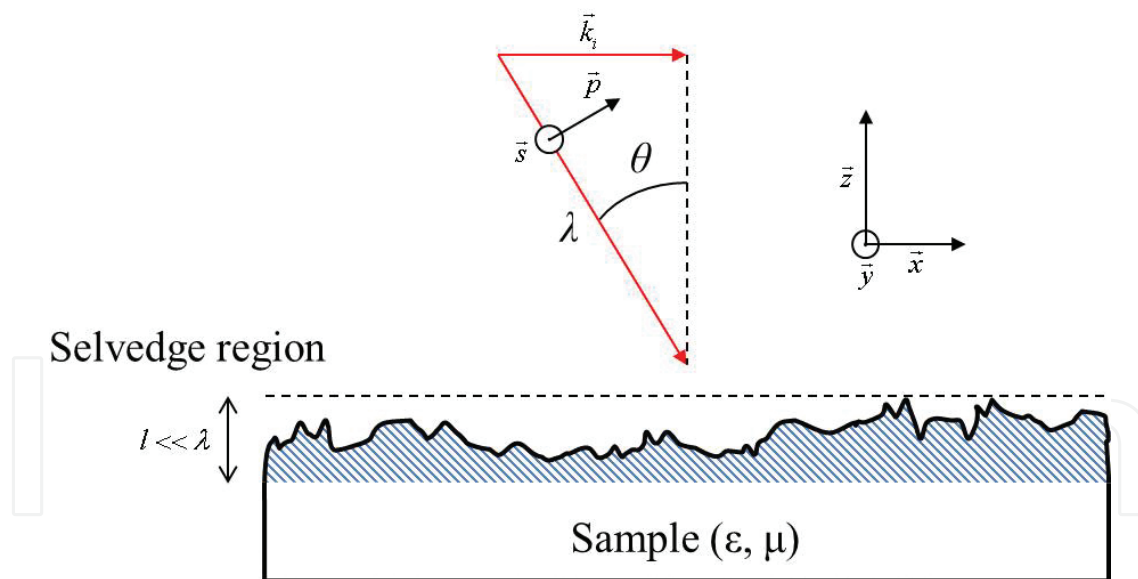


**Figure 1.** Geometry of a one-dimensional rough surface of length  $L$ . The medium below the rough interface is electrically defined by the permittivity  $\epsilon$  and permeability  $\mu$ . The surface roughness is assumed to be confined in a “selvedge region” in a range between  $z = 0$  and  $z = 1$ , where  $1 \ll \lambda$ .

Discussion of a contribution of surface plasmon polaritons has been presented by Bonse et al. [71, 72] and Miyaji et al. [58, 59], where the formation of LSFL and HSFL was experimentally observed with the change of optical properties induced by an electron excitation under laser irradiation. Huang et al. showed that self-organized LSFL on dielectric materials was formed

via a metallic-like behavior by an interference of initial surface plasmon and laser pulses followed by the grating assisted surface plasmon-laser coupling [67]. They also obtained a good agreement with their experimental results, by taking account into the effect of surface plasmon. Reif et al. reported that HSFL is due to self-organization structure formation during the relaxation of highly non-equilibrium condition after explosive ion emission [63]. Straub et al. demonstrated that generation of a dense electron-hole plasma at a carrier concentration slightly beyond the critical plasma density allows for the excitation of surface plasma waves at the high-spatial frequencies that are required for HSFL formation [60]. Bonse et al. explained HSFL formation based on the interference between the surface-scattered wave of the laser and its second harmonic [57, 71, 73]. Okumuro et al. found that the periodicity of HSFL can be explained by induction of a surface-plasma wave through the parametric process of laser light [69]. They also showed that laser fluence dependence of periodic grating structures was formed on metal surfaces under femtosecond laser pulse irradiation. The results indicate that the formation of periodic grating structures depends not only on target properties but also on the electron density of plasma produced in the femtosecond excitation regime [70].

## 2.2. Surface microstructures in higher energy regime

Femtosecond laser machining with high fluence can selectively remove large volumes of material only in the focal area. Thermal effect could be observed in higher fluence more than the threshold value of materials even though heat diffusion outside the focal area is comparatively minimized in contrast to longer pulse lasers. Several literatures have provided evidence for the existence of a molten region surrounding ablation area, even for the ultrashort pulse processing [39–41, 74]. Thermocapillary force and hydrodynamic force will be dominated in the high-fluence regime. Theoretical model for the regime has also been fabricated and seems to be in good agreement with experimental results [41]. Yaker et al. showed reliable evidence regarding the formation mechanism of surface microstructure induced by high-fluence femtosecond pulses. They tried to fabricate a microflow channel for microfluidic devices by scanning femtosecond laser beam on a borosilicate glass. The experiment was performed by mutually overlapping thin rims surrounding the laser-induced smooth crater to produce surface microstructures as shown in **Figure 2**.

The crater surrounded by thin rim is created by resolidification of a molten layer generated during the ablation process. They found that a thin rim is formed around the craters and is created on the undamaged surface. To investigate the mechanism of granulated rim formation by successive laser pulses, they also demonstrated theoretical analysis of the thermal and fluid processes taking into account ablation process in the femtosecond regime. The series of the experiment indicate that a thin molten layer below the surface and the rim is generated by the high pressure resulted from a dense plasma producing a pressure-driven fluid motion of the molten material outwards from the center of laser focal point as shown in **Figures 2** and **3**. The second laser pulse is diffracted by the rim created by the first laser pulse, resulting in diffraction pattern on the crater area overlapped. The distance between the diffraction rims seems to be approximately equal to the wavelength of the laser light, which means that diffraction by the rim plays an important role for the formation of granulated structures. Flow forces applied to

a molten layer are generated from expanding plasma which can be happened by thermocapillary forces and forces driven by plasma expansion above the irradiated surface. There are a number of processes in the regime of femtosecond pulse-induced phenomena, including nonlinear absorption, plasmas, shock propagation, melt propagation, and resolidification. These processes can roughly be broken down into three different time domains as illustrated in **Figure 4**.

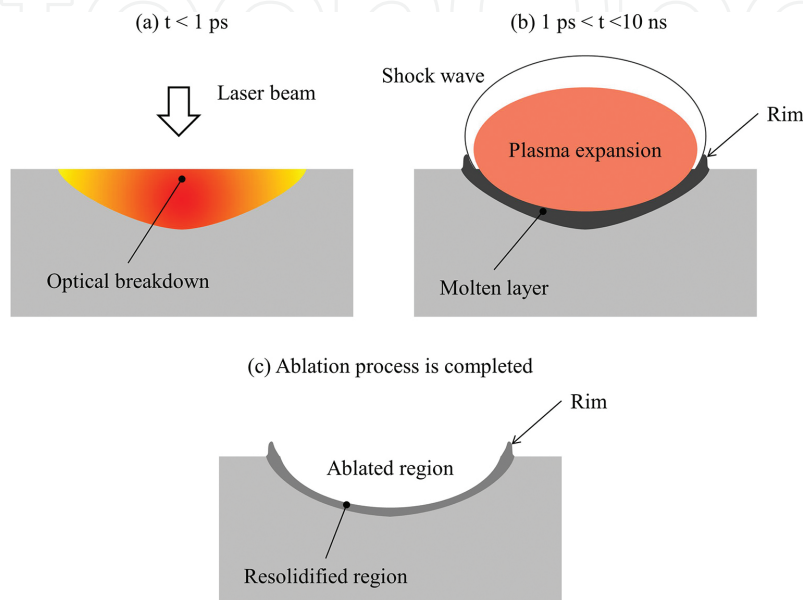


**Figure 2.** A schematic of ablation process with a femtosecond laser pulse in the characteristic time (a)–(c) of excitation and relaxation process.

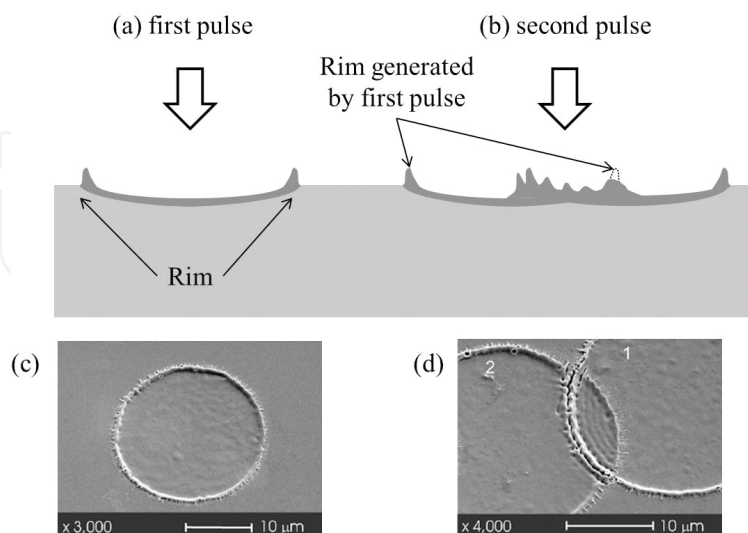


**Figure 3.** Femtosecond laser-induced crater rim and its diffraction pattern generated by overlapping two pulses. (a), (c) One laser pulse. (b), (d) Two overlapping pulses. (SEM pictures adapted with permission from Ref. [41], © IOP Publishing. Reproduced by permission of IOP Publishing. All rights reserved).

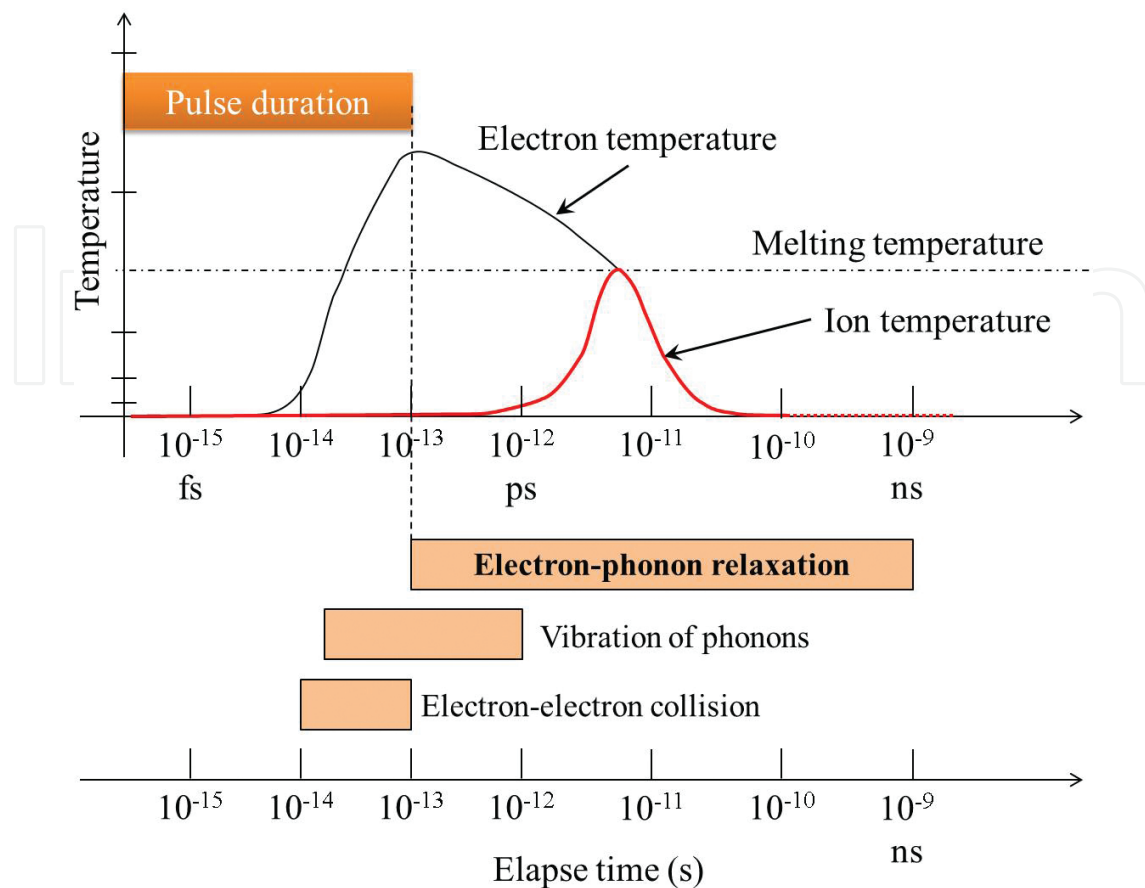


**Figure 4.** Characteristic time of excitation and relaxation process.

The physics and discussions mentioned in this section are quite important for the case of using femtosecond laser microstructuring into microdevices such as a thin optical fiber to be highly functionalized. The following sections show the functionalization of optical fibers using femtosecond laser drilling, the operation of which requires a large number of pulses, and high fluence much larger than a material threshold to fabricate 3D microstructures. The surface-granulated structures found in the above approach are also discussed with recent experimental results in our research groups.

### 3. Femtosecond laser hole drilling to optical fibers

In the past three decades, fiber-optic sensor technology has been developed for different applications. The progresses in research have developed the fiber-optic sensors for practical applications. For instance, distributed fiber-optic sensors have been installed in dams and bridges to monitor the performance of these facilities. With the rapid growth of optical networks, the cost of fiber-optic sensors has significantly decreased as key components in fiber-optic sensors (such as optical fiber, light sources, and photo detectors) are commercially available in optical communications industries. Therefore, it can be anticipated that fiber-optic

sensors will be used in more extensive applications in sensing technology. Recent interest in the technologies has not only been focused on the development of novel ideas but also on technologies for integrating high-performance devices of various functionalities onto a single optical fiber, which are sometimes referred to as “lab-on-fiber” technologies. The authors have previously reported a new approach to the development of a fiber-optic spectrometer by embedding a microhole to be a spectroscopic sample cell in multimode optical fiber, using a near-ultraviolet (NUV) femtosecond laser [22].

Optical fiber sensors machined by femtosecond laser drilling are summarized in **Table 1**. The fiber-optic sensor with a microhole working as a sensing area in single-mode optical fibers [19, 20] was demonstrated to monitor the refractive index (RI) of liquid, in which the microhole structures were fabricated by femtosecond laser irradiation of near infrared (NIR) at 800 nm with a 120-fs duration pulse at 1 kHz repetition rate during 15 s and pulse energy of 11  $\mu\text{J}$ . The sensor performances seem to be limited for introducing liquid into the microhole when using high viscous liquids because the shapes of microholes are sharply tapered over the entire hole due to objective lens used to focus laser beam and its fabrication procedure of one side laser irradiation. The other experiment [21] was conducted by using 1030-nm NIR femtosecond laser with a 280-fs pulse of pulse energy of 1–5  $\mu\text{J}$  and 100-kHz high repetition rate during 5 min, and immersion oil is also required to reduce the laser-induced thermal energy. An optical fiber was immersed in water to avoid the thermal influence, where helical drilling method was also employed in the fabrication procedure in order to reduce tapering the microhole. However, the tapering in the lateral direction of optical axis still remains at the opposite side of cladding because laser beam is focused by passing through the cylindrical body of the optical fiber processed. For the case of femtosecond laser deep drilling to dielectrics, laser energy can be nonlinearly transferred to electrons via multiphoton absorption, where the order of N-photon ionization process is determined by photon energy. This fact indicates that ablation threshold becomes lower with decreasing wavelength [75, 76] because efficient energy transfer to electrons can be easily achieved via a shorter-wavelength femtosecond laser via efficient multiphoton absorption with reducing extra energy diffusion by collision cascade [77, 78]. Consequently, it can be supposed that a shorter-wavelength laser with a higher photon energy is comparatively favorable for microstructuring in microscale platforms such as thin optical fibers because the shorter-wavelength beam can reduce thermal debris inevitably generated through resolidification of a molten material. Such debris disturbs growth of microhole by absorbing/scattering subsequent laser pulses and redeposition of debris on the hole surface, resulting in poor surface quality of the inner wall. Actually, the experiment conducted on the fabrication of microhole with 1030-nm femtosecond laser in air atmosphere was tested experimentally and failed [21]. Moreover, it was found that the surface microstructures on the inner wall are remarkably different between using NIR and NUV femtosecond laser drilling. Further advantage of use of 400-nm laser deep drilling is found in the fact that Rayleigh range can be longer. In contrast to the hole drilling using NIR wavelength (e.g. 800 nm [19, 20], 1030 nm [21]) which were inevitably accompanied with debris and longer processing period more than 10 s or 5 min, efficient deep hole drilling in glass optical fiber was successfully demonstrated with reducing debris in a very short irradiation time of approximately 1.0 s to fabricate a fiber-optic inline spectrometers, using a 400-nm, 1-kHz, and 350-fs laser irradiation.

Laser and its irradiation condition							Cell					
References	Pulse width (fs)	Wave length (nm)	Repet- ition (kHz)	Pulse energy ( $\mu\text{J}$ )	Irradi- ation time (s)	Fabric- ation process	Lens NA	Number of hole	Shape (taper angle)	Hole diameter ( $\mu\text{m}$ )	Roughness	Volume (single cell) (pL)
[19]	120	800	1	11 $\mu\text{J}$	5 s 10 s 15 s	Single direction	0.25	1	Dead-end ( $7^\circ\text{--}10^\circ$ )	6 8 11	–	1.2 6.3 12
[20]	–	–	–	–	–	–	–	1	Through hole ( $4^\circ\text{--}18^\circ$ )	15	>3 $\mu\text{m}$	60–80
[21]	280	1030	100	1–5 $\mu\text{J}$	5 min	Helical drilling	0.68	SM: 1 MM: 3	Through hole ( $1^\circ\text{--}4^\circ$ )	20	300 nm (no evidence)	40
[22]	350	400	1	15 $\mu\text{J}$	1.2 s	Two direction	0.40	MM: 1, 10	Through hole ( $3.7^\circ$ )	10	<500 nm	20

**Table 1.** Optical fiber sensors with a microhole produced by femtosecond laser drilling.

### 3.1. Fabrication of microholes into optical fibers

The following sections show results obtained in our recent study regarding the fabrication of optical fiber sensors using femtosecond laser with high-fluence regimes. As shown in **Figures 5** and **6**, the microholes are intentionally designed and machined to easily guide a liquid sample into microhole working as a sensing area without immersion liquids during fabrication process. The sensor part has microhole array penetrating through the whole fiber core by drilling from both sides of the fiber cladding in order to avoid tapering the opening apertures inlet/outlet of through hole.

The microholes were fabricated with optical train, as illustrated in **Figure 5**. A multimode optical fiber (MMF, core diameter 62.5  $\mu\text{m}$ ) was irradiated with femtosecond pulses from two directions (not simultaneously) to avoid tapering of the inlet/outlet of the cell. The fundamental of a 1 kHz Ti-sapphire laser (IFRIT Cyber Laser Inc., 1 mJ/pulse,  $\lambda = 800$  nm, 210 fs pulse duration) was converted to the second harmonic (240  $\mu\text{J}$ /pulse, 350 fs pulse duration) in a wavelength converter [second harmonic generation (SHG) unit, manufactured by Cyber Laser Inc.]. The second harmonic pulses were introduced to an objective lens through an optical train to guide and focus the beam at the target optical fiber. The collimating optics reduce the beam diameter from 6.0 to 2.8 mm so that a longer Rayleigh distance compared with the initial beam can be obtained using a negative and positive lens array. This prevents plasma generation in the air between the lens combination, which is important because the laser beam could be defocused and the energy could be lost by plasma creation during collimation and thereby affected by diffraction before the final focusing. An optical fiber irradiated was mounted on a three-dimensional motor-controlled translation stage equipped with a rotary mechanism for

rotation of the fiber. The laser focal point was carefully adjusted by moving the translation stage in the X, Y, Z, and  $\theta_x$  directions. The focal point, defined as the center of the Rayleigh distance, was set to be 5  $\mu\text{m}$  beyond the cladding surface of the inlet.

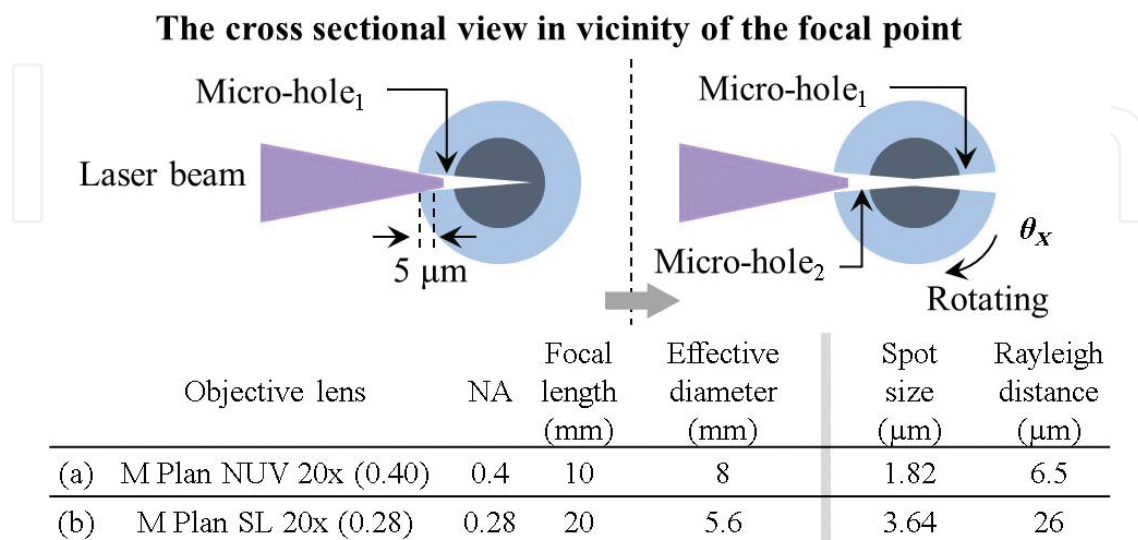


**Figure 5.** The cross-sectional view in vicinity of the focal point and two different types of collimations.

### 3.2. Surface roughness on inner wall

**Figure 6(a)** and **(b)** indicates the schematic images of side and cross-sectional views of the through holes embedded in optical fiber lines, respectively. Based on the microscopic image showing the fabricated through hole **(c)**, the hole diameters were found to be approximately 18 and 10  $\mu\text{m}$  at the opening aperture and waist, respectively, the volume of which was calculated to 19.8 pL by assuming that its shape could be approximated by two truncated cones with taking into account the taper angle of the microhole. Optical micrographs of the through hole of the side and top view are presented in **Figure 6(c)** and **(d)**, respectively, showing that the microholes are connected together so as to produce a through hole. Taking a look at the inside of the through hole by using scanning electron microscope (SEM) as shown in **Figure 6(e)**, a morphology modification was formed to be granulated structure, which have been reported so far in the previous works as mentioned above in the femtosecond regime [41]. The sample of **Figure 6(e)** was prepared in such a way that the inner surface of a part of hole was exposed by intentionally cleaving the fabricated fiber along an off-axis plane of the through hole to clearly see the rugged surface with SEM. The rough surface could be generated with folded debris or microrims surrounding laser-induced craters by successive laser pulses. Importantly, the size of the rugged particle is found to be approximately a few hundred nanometers. Such rough surface gives more diffusive reflection on the hole boundary, hence higher optical scattering, especially for shorter-wavelength light wave. Additionally, it should also be noted that such particle-like structure will be more water repellent to a liquid by which water inside becomes easier to flow. As shown in **Table 1**, the surface roughness should be depended on the fabrication method. The shorter wavelength laser irradiation can reduce the

increasing thermal debris and its redeposition on the inner surface, the fact of which can be seen from the comparison between Refs. [20] and [22].

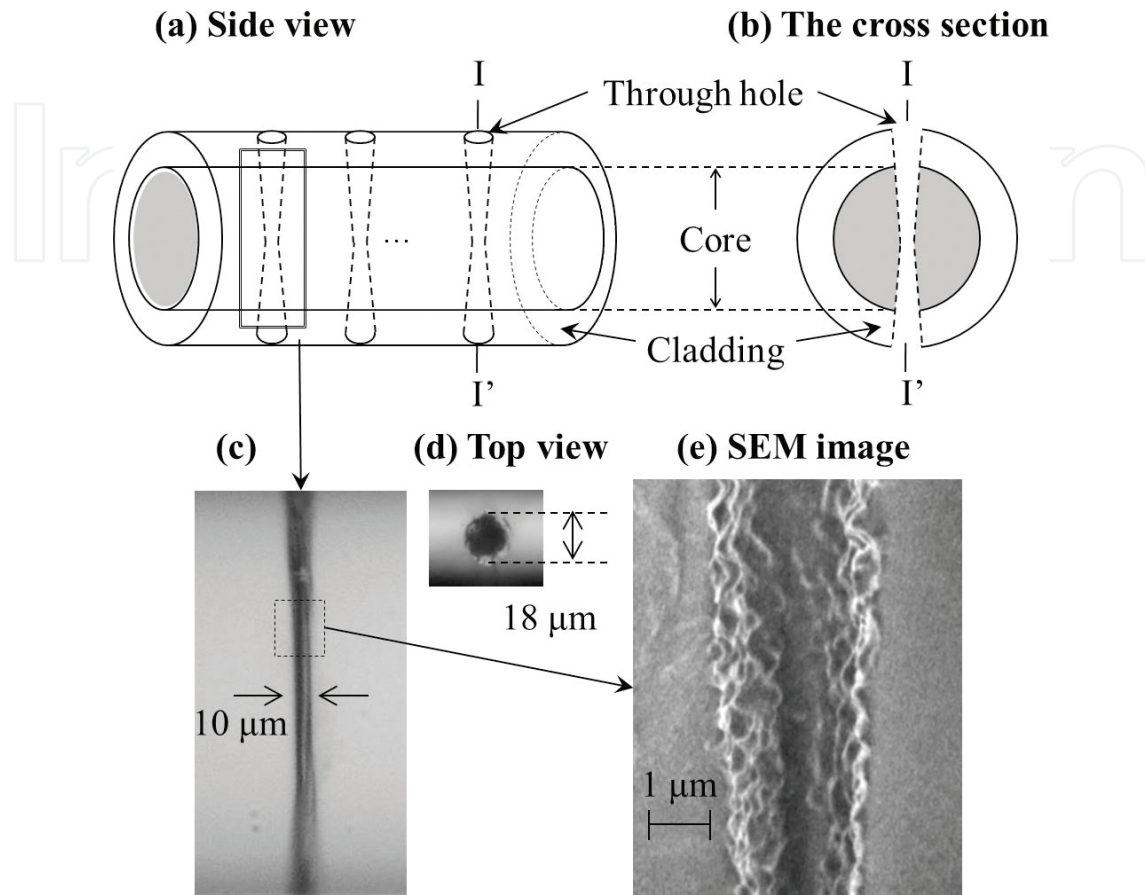


**Figure 6.** The schematic drawings of microholes in a fiber-optic line monitored from side view (a) and the cross section (b). The photographs of (c) and (d) give examples which show the shape of the through hole and the hole opening, respectively. (e) SEM picture of a part of hole. Adapted with permission from Ref. [22].

### 3.3. Influences of surface roughness for sensing

To evaluate the intrusion/discharge velocity of liquids sucked into/drained out from a through hole, the real-time response of optical intensity change was measured in such a way that the sensing part with a single through hole is alternatively immersed in water and ethanol as indicated in **Figure 7**. Sample liquids were immediately sucked into microholes by capillary driving force and as was firstly confirmed by monitoring the optical intensity of transmitting light and staining the microhole with a color dye simultaneously. As soon as the sensing part was lifted from a liquid pool, the liquid held in the microhole seems to be immediately drained out in a few seconds because of the hydrophobic-repellent structure.

**Figure 8** shows transmitting spectra to investigate sensing response for RI changes in a wavelength between 400 and 1000 nm. In this measurement, two types of sensor samples which had (a) a single cell and (b) 10 cells were prepared to compare the spectroscopic measurement

between them. Taking a look at **Figure 8(b)**, remarkable decreases in transmission can be confirmed in a shorter wavelength range ( $\lambda < 600$  nm), because light transmitted through the fiber core was scattered at the hole surfaces by the fact that the wavelength of transmitted light becomes approximately equal to the scale of surface roughness. By reducing or controlling the surface roughness on the inner wall, sensing performances of fiber optics with an inline sample cell in terms of sensitivity, reproducibility, response time, and recovery time as well as versatility for sensing target could be improved for practical use. High-quality surface finish therefore is required for the improvement of the sensing performances even in high-fluence regimes. The roughness with a periodicity of  $<100$  nm could be useful for reducing the scattering in a shorter wavelength range, by roughly estimating the reflectivity on the inner wall based on Mie-scattering effect.

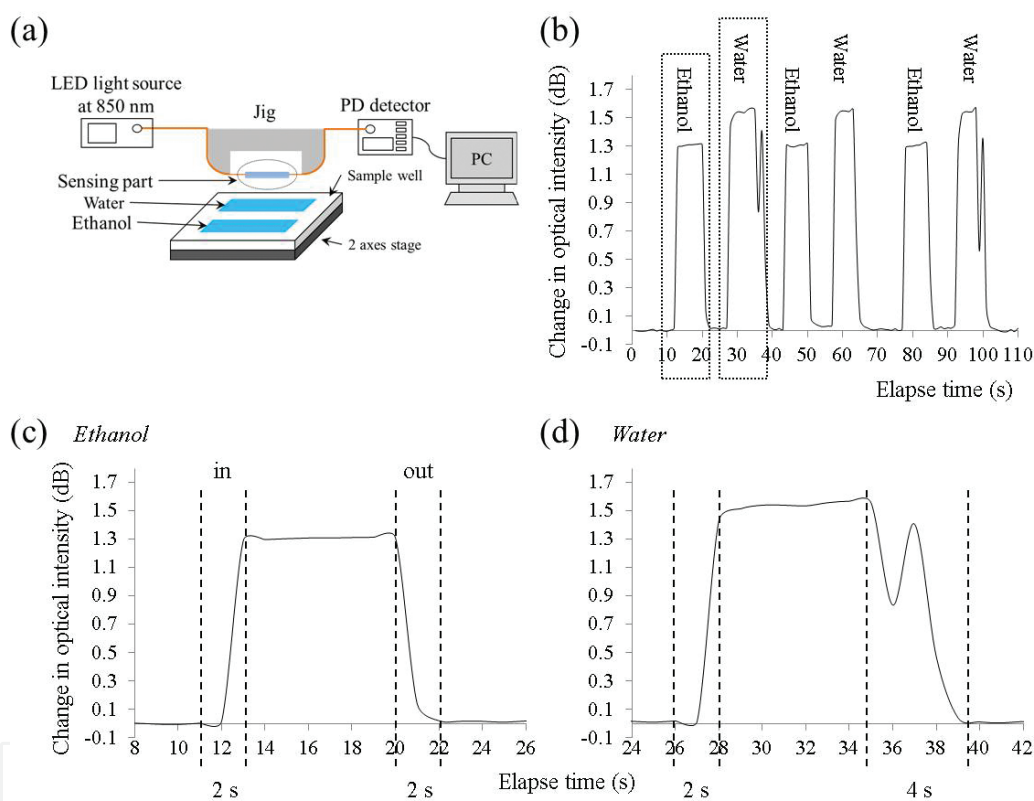


**Figure 7.** (a) Experimental setup to measure intrusion/discharge velocity of liquids. (b) The real-time response of optical intensity change measured by alternatively immersing in water and ethanol. (c) and (d) show one of a response waveform using ethanol and water, respectively.

According to the experimental data [19–22] (summarized in **Table 1**), the roughness might be reduced by immersing an optical fiber in water or immersion oils even though the fabrication period becomes unfavorably much longer. Instead of using liquid immersion processing, we have been trying to reduce the roughness using a NUV 400-nm femtosecond laser so as to achieve a high-quality inner surface of microhole in a high-throughput fashion. **Figure 9** shows SEM pictures of the inner surface of a dead-end microhole fabricated in a flat silica glass plate. The experiment was performed to make a smooth surface on the inner wall of the hole with

varying laser irradiation parameters. As can be seen from **Figure 9(a)**, wave-like nanostructures with a spatial periodicity of 100–200 nm are observed on the bottom of the hole. **Figure 9(b)** and **(c)**, respectively, shows the inner surface of the hole at different depths near and far from the hole inlet. Surface roughness is still observed at the periphery of the inlet of **Figure 9(b)** because the surface roughness could be worse as the number of irradiated pulses becomes greater. On the other hand, the case of the inner surface **Figure 8(c)** seems to be much smoother than the surface (b). To figure out the formation mechanism of the granulated surface in a high-energy regime, further experiment was carried out on this point.

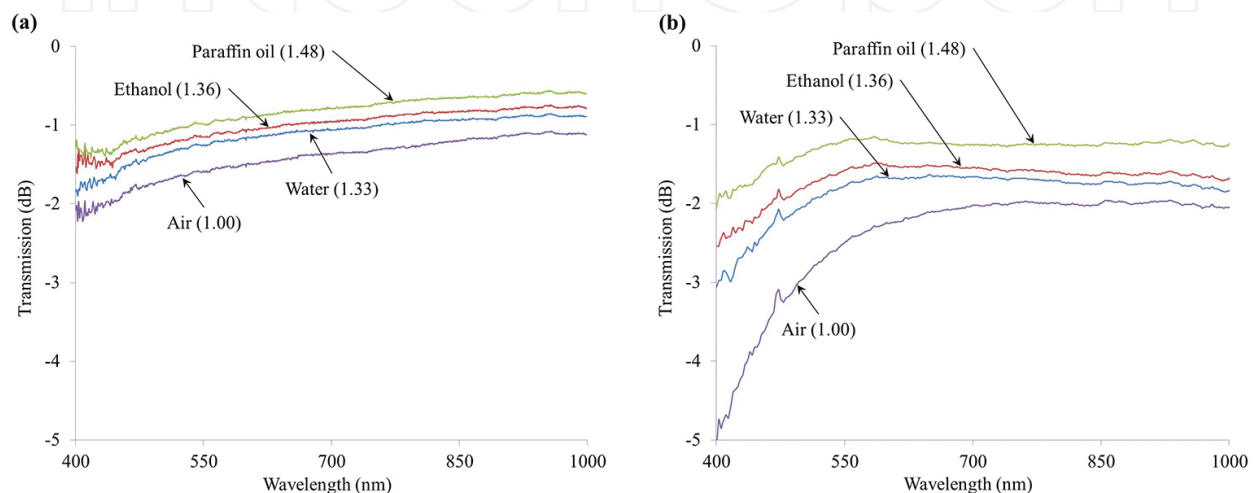


**Figure 8.** Transmission spectra for the case of sensor samples (a) single cell and (b) 10 cells when immersion in three types of liquids. Adapted with permission from Ref. [22].

The surface morphology of shallow craters was generated by single and multiple pulses with an emphasis on rims surrounding the craters. In this experiment, shallow craters were formed on a fused silica plate by overlapping focused laser pulses on the same spot as shown in **Figure 10**. The shape of the crater created in this experiment is depended on incident laser beam, the pattern of which is deformed through a second harmonic generator (SHG unit manufactured by Cyber Laser Inc.). A crater surrounded by a single rim was observed by SEM analysis of **Figure 11(b)**. The average thickness of the first rim is approximately 500 nm. **Figure 11(c)** shows an overlapped crater created by two pulses. Molten materials are driven away from the crater to almost 10  $\mu\text{m}$  distance. The second image (**Figure 11(d)**) shows that a new rim is formed inside the first one by overlapping a second pulse. The distance between the two rims is approximately equal to the wavelength of the irradiated laser beam. We also found a belt-shape structure on a part of the rim. The composition and formation mechanism still need to be explored. For the case of **Figure 11(f)**: overlapping three pulses, it was interestingly found that the height of third rim is comparatively low simultaneously accompanied with nanofibers [79–81] with a diameter ranging from a few to few tens of nanometers. It should be noted that, instead of the growth of the rim, nanofibers were grown by only a few pulses. In order to obtain optimum surface conditions for the fiber-optic inline spectrometer, further investigations are in progress to improve the surface finish.

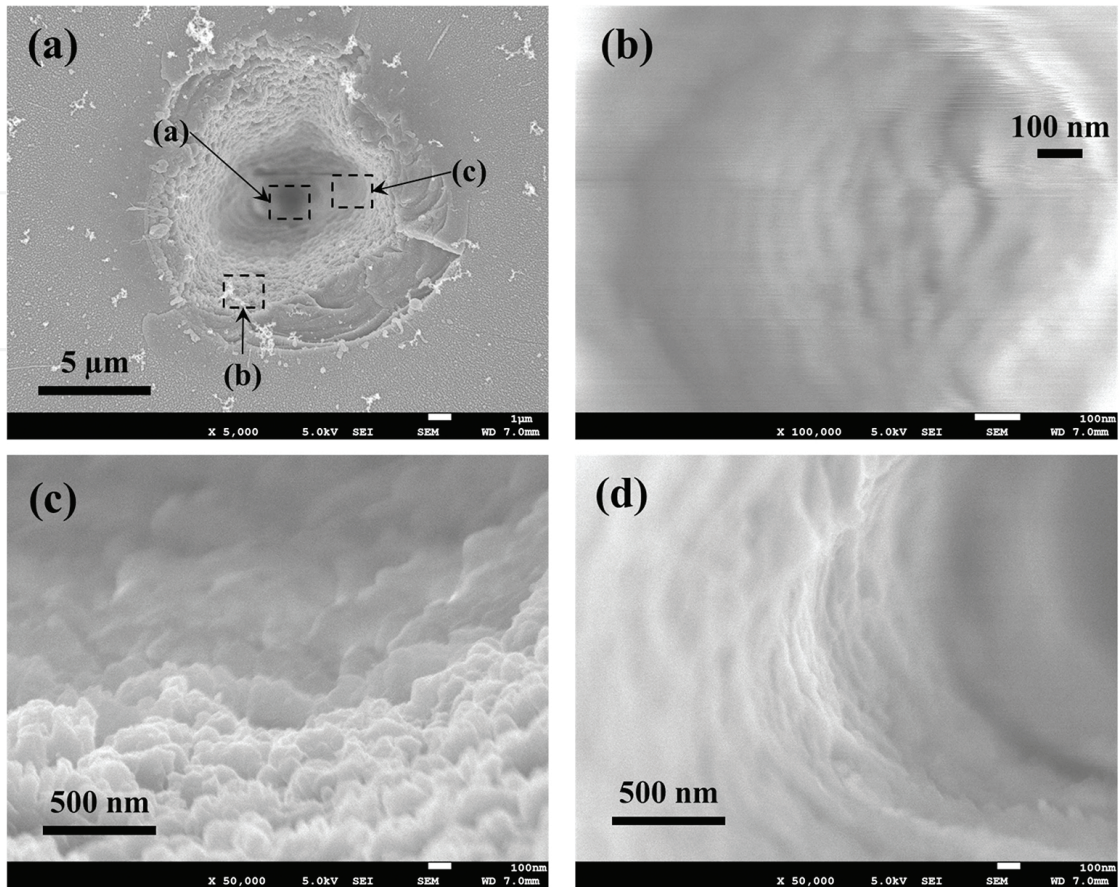


**Figure 9.** SEM images of a microhole generated on a flat silica glass plate, by successive laser pulses of the energy of  $20 \mu\text{J}$  and using focusing optics (inserted table (b) in **Figure 5**). (a) The whole fabricated microhole at  $5000\times$  magnification and higher resolution SEM pictures at hole bottom (b), the side wall near the hole inlet (c), and the side wall near the bottom (d).

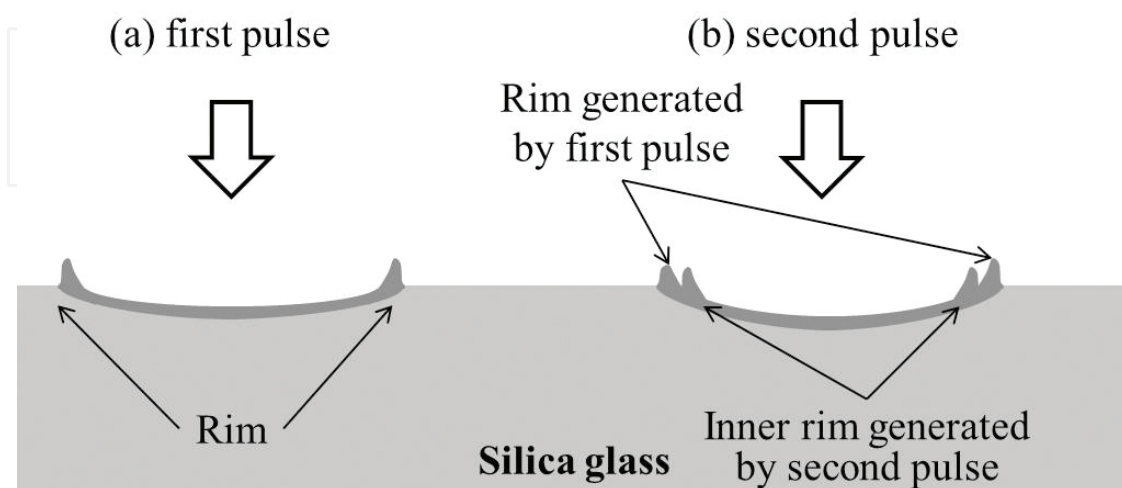


**Figure 10.** The schematic image of crater rims produced by overlapping focused laser pulses on the same spot. (a) One laser pulse. (b) Two overlapping pulses.

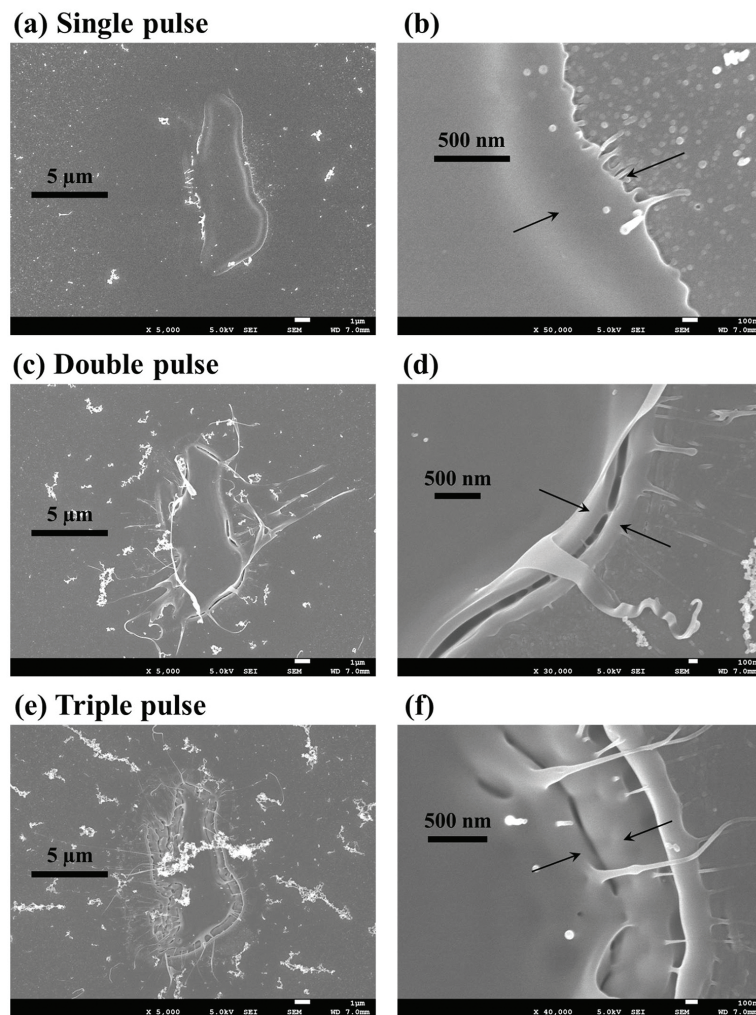


**Figure 11.** SEM images of shallow craters with thin rim generated on a flat silica glass plate with varying the number of pulses. The whole crater at 5000 $\times$  magnification (a, c, e) and higher resolution (b, d, f).

#### 4. Conclusion

In this chapter, the authors presented an overview of laser-induced periodic surface structures (LIPSS) produced by ultrashort laser pulses. A part of its historical background was provided; the formation mechanism of LIPSS in femtosecond pulse regimes was described. Experimental results obtained by our studies were also presented as a practical use of femtosecond micro-machining even though a part of the result is still under investigation.

Section 4 shows the functionalization of optical fibers using femtosecond laser drilling. High-fluence femtosecond laser microstructuring was described with recent experimental data in our research group. The investigation not only to explain the formation mechanism of LIPSS but also to have a microscale perspective should be important for material removal because a high-throughput fabrication of 3D microstructures to microdevices requires a large number

of pulses and high fluence. We therefore expect that the obtained results can contribute to practical aspects.

## Acknowledgements

This work has been partially supported by JSPS KAKENHI Grant Number 15K04735.

## Author details

Kenji Goya<sup>1\*</sup>, Masahiko Shiraishi<sup>2</sup>, Yusuke Fuchiwaki<sup>1</sup>, Kazuhiro Watanabe<sup>2</sup> and Toshihiko Ooie<sup>1</sup>

\*Address all correspondence to: k-gouya@aist.go.jp

1 National Institute of Advanced Industrial Science and Technology (AIST), Hayashi-cho, Takamatsu, Kagawa, Japan

2 Soka University, Tangi-machi, Hachioji, Tokyo, Japan

## References

- [1] S.S. Mao, F. Qu'er', S. Guizard, X. Mao, R.E. Russo, G. Petite, P. Martin, Dynamics of femtosecond laser interactions with dielectrics, *Appl. Phys. A Mater. Sci. Process.* 79 (2004) 1695–1709. doi:10.1007/s00339-004-2684-0.
- [2] S. Kanehira, K. Miura, K. Hirao, Ion exchange in glass using femtosecond laser irradiation, *Appl. Phys. Lett.* 93 (2008) 2–4. doi:10.1063/1.2959820.
- [3] Y. Liao, Y. Shen, L. Qiao, D. Chen, Y. Cheng, K. Sugioka, K. Midorikawa, Femtosecond laser nanostructuring in porous glass with sub-50 nm feature sizes., *Opt. Lett.* 38 (2013) 187–189. doi:10.1364/OL.38.000187.
- [4] B.N. Chichkov, C. Momma, S. Nolte, F. von Alvensleben, A. Tuinnermann, Femtosecond, picosecond and nanosecond laser ablation of solids, *Appl. Phys. A Mater. Sci. Process.* 115 (1996) 109–115.
- [5] D. Vipparty, B. Tan, K. Venkatakrisnan, Nanostructures synthesis by femtosecond laser ablation of glasses, *J. Appl. Phys.* 112 (2012) 073109:1–7. doi:10.1063/1.4754864.
- [6] G. Dumitru, V. Romano, H.P. Weber, M. Sentis, W. Marine, Femtosecond ablation of ultrahard materials, *Appl. Phys. A Mater. Sci. Process.* 74 (2002) 729–739. doi:10.1007/s003390101183.

- [7] K. Furusawa, K. Takahashi, H. Kumagai, K. Midorikawa, M. Obara, Ablation characteristics of Au, Ag, and Cu metals using a femtosecond Ti: sapphire laser, *Appl. Phys. A Mater. Sci. Process.* 69 (1999) S359–S366. doi:10.1007/s003399900393.
- [8] S. Ahsan, Y. Gyu, M. Seop, Formation mechanism of nanostructures in soda – lime glass using femtosecond laser, *J. Non. Cryst. Solids.* 357 (2011) 851–857. doi:10.1016/j.non-crysol.2010.11.006.
- [9] Y. Guan, C. Li, X. Cheng, B. Wang, R. Sun, X. Liang, J. Zhao, H. Chen, G. Lu, Highly sensitive mixed-potential-type NO<sub>2</sub> sensor with YSZ processed using femtosecond laser direct writing technology, *Sensors Actuators, B Chem.* 198 (2014) 110–113. doi:10.1016/j.snb.2014.02.098.
- [10] X. Zhao, Y.C. Shin, Femtosecond laser drilling of high-aspect ratio microchannels in glass, *Appl. Phys. A Mater. Sci. Process.* 104 (2011) 713–719. doi:10.1007/s00339-011-6326-z.
- [11] Y. Shimotsuma, H. Kazuyuki, P.G. Kazansky, J. Qiu, Invited Review Paper Three-Dimensional Micro- and Nano-Fabrication in Transparent Materials by Femtosecond Laser, 44 (2005) 4735–4748. doi:10.1143/JJAP.44.4735.
- [12] M. Barberoglou, V. Zorba, E. Stratakis, E. Spanakis, P. Tzanetakis, S.H. Anastasiadis, C. Fotakis, Bio-inspired water repellent surfaces produced by ultrafast laser structuring of silicon, *Appl. Surf. Sci.* 255 (2009) 5425–5429. doi:10.1016/j.apsusc.2008.07.130.
- [13] C. Hnatovsky, R.S. Taylor, E. Simova, P.P. Rajeev, D.M. Rayner, V.R. Bhardwaj, P.B. Corkum, Fabrication of microchannels in glass using focused femtosecond laser radiation and selective chemical etching, *Appl. Phys. A.* 84 (2006) 47–61. doi:10.1007/s00339-006-3590-4.
- [14] M. Duocastella, J.M. Fernández-Pradas, J.L. Morenza, D. Zafra, P. Serra, Novel laser printing technique for miniaturized biosensors preparation, *Sensors Actuators, B Chem.* 145 (2010) 596–600. doi:10.1016/j.snb.2009.11.055.
- [15] C. Cugnet, O. Zaouak, A. René, C. Pécheyran, M. Potin-Gautier, L. Authier, A novel microelectrode array combining screen-printing and femtosecond laser ablation technologies: development, characterization and application to cadmium detection, *Sens. Act. B Chem.* 143 (2009) 158–163. doi:10.1016/j.snb.2009.07.059.
- [16] M. Yamaji, H. Kawashima, J. Suzuki, S. Tanaka, Three dimensional micromachining inside a transparent material by single pulse femtosecond laser through a hologram, *Appl. Phys. Lett.* 93 (2008) 041116:1–3.
- [17] I. Sohn, Y. Kim, Y. Noh, I.W. Lee, J.K. Kim, H. Lee, Femtosecond laser and arc discharge induced microstructuring on optical fiber tip for the multidirectional firing, *Opt. Express.* 18 (2010) 19755–19760. doi:10.1364/OE.18.019755.
- [18] C.H. Chen, T.C. Tsao, W.Y. Li, W.C. Shen, C.W. Cheng, J.L. Tang, C.P. Jen, L.K. Chau, W. Te Wu, Novel U-shape gold nanoparticles-modified optical fiber for localized plasmon

resonance chemical sensing, *Microsyst. Technol.*, 2010: pp. 1207–1214. doi:10.1007/s00542-009-0945-8.

- [19] Y. Wang, D.N. Wang, M. Yang, W. Hong, P. Lu, Refractive index sensor based on a microhole in single-mode fiber created by the use of femtosecond laser micromachining, *Opt. Lett.* 34 (2009) 3328–3330. <http://www.ncbi.nlm.nih.gov/pubmed/19881583>.
- [20] Y. Wang, M. Yang, D.N. Wang, S. Liu, P. Lu, Fiber in-line Mach–Zehnder interferometer fabricated by femtosecond laser micromachining for refractive index measurement with high sensitivity, *J. Opt. Soc. Am. B.* 27 (2010) 370–374. doi:10.1364/JOSAB.27.000370.
- [21] R. Buividas, M. Mikutis, G. Gervinskas, D. Day, G. Sleky, S. Juodkasis, Femtosecond laser drilling of optical fibers for sensing in microfluidic applications, In: *Proc. SPIE – Int. Soc. Opt. Eng.*, 2012: p. 84630T. doi:10.1117/12.929607.
- [22] K. Goya, T. Itoh, A. Seki, K. Watanabe, Efficient deep-hole drilling by a femtosecond, 400 nm second harmonic Ti: Sapphire laser for a fiber optic in-line/pico-liter spectrometer, *Sensors Actuators, B Chem.* 210 (2015) 685–691.
- [23] Z. Tian, S.S. Yam, H. Loock, Refractive index sensor based on an abrupt taper Michelson interferometer in a single-mode fiber, 33 (2008) 1105–1107.
- [24] F.C. Favero, L. Araujo, G. Bouwmans, V. Finazzi, J. Villatoro, V. Pruneri, Spheroidal Fabry-Perot microcavities in optical fibers for high-sensitivity sensing, *Opt. Express.* 20 (2012) 7112. doi:10.1364/OE.20.007112.
- [25] Y.-J. Rao, M. Deng, D.-W. Duan, X.-C. Yang, T. Zhu, G.-H. Cheng, Micro Fabry-Perot interferometers in silica fibers machined by femtosecond laser, *Opt. Express.* 15 (2007) 14123–14128. doi:10.1364/OE.15.014123.
- [26] F. Müller, C. Kunz, S. Gräf, Bio-inspired functional surfaces based on laser-induced periodic surface structures, *Materials (Basel)*. 9 (2016) 476. doi:10.3390/ma9060476.
- [27] M. Yamaguchi, Y. Kaneko, M. Sasaki, Fabrication of nano-periodic structure on plastic film for water repellent using femtosecond laser, *Transaction on Control and Mechanical Systems* 1 (2012) 306–311.
- [28] M.R. Cardoso, V. Tribuzi, D.T. Balogh, L. Misoguti, C.R. Mendona, Laser microstructuring for fabricating superhydrophobic polymeric surfaces, *Appl. Surf. Sci.* 257 (2011) 3281–3284. doi:10.1016/j.apsusc.2010.10.156.
- [29] A.Y. Vorobyev, C. Guo, Multifunctional surfaces produced by femtosecond laser pulses, *J. Appl. Phys.* 117 (2015) 033103:1–5. doi:10.1063/1.4905616.
- [30] J. Hiller, J.D. Mendelsohn, M.F. Rubner, Reversibly erasable nanoporous anti-reflection coatings from polyelectrolyte multilayers, *Nat. Mater.* 1 (2002) 59–63. doi:10.1038/nmat719.

- [31] S.-H. Hong, B.-J. Bae, K.-S. Han, E.-J. Hong, H. Lee, K.-W. Choi, Imprinted moth-eye antireflection patterns on glass substrate, *Electron. Mater. Lett.* 5 (2009) 39–42. doi:10.3365/eml.2009.03.039.
- [32] K. Han, J. Shin, H. Lee, Enhanced transmittance of glass plates for solar cells using nano-imprint lithography, *Sol. Energy Mater. Sol. Cells.* 94 (2010) 583–587. doi:10.1016/j.solmat.2009.12.001.
- [33] S. Liu, C. Liao, Fast fabrication of nano-structured anti- reflection layers for enhancement of solar cells performance using plasma sputtering and infrared assisted roller embossing techniques, 20 (2012) 2908–2912.
- [34] A.A. Ionin, Y.M. Klimachev, A.Y. Kozlov, S.I. Kudryashov, A.E. Ligachev, S. V. Makarov, L. V. Seleznev, D. V. Sinitsyn, A.A. Rudenko, R.A. Khmel'nitsky, Direct femtosecond laser fabrication of antireflective layer on GaAs surface, *Appl. Phys. B Lasers Opt.* 111 (2013) 419–423. doi:10.1007/s00340-013-5350-4.
- [35] N. Tagawa, M. Takada, A. Mori, H. Sawada, K. Kawahara, Development of contact sliders with nanotextures by femtosecond laser processing, *Tribol. Lett.* 24 (2006) 143–149. doi:10.1007/s11249-006-9142-4.
- [36] A.A. Voevodin, J.S. Zabinski, Laser surface texturing for adaptive solid lubrication, *Wear.* 261 (2006) 1285–1292. doi:10.1016/j.wear.2006.03.013.
- [37] K.J. Kubiak, M.C.T. Wilson, T.G. Mathia, P. Carval, Wettability versus roughness of engineering surfaces, *Wear.* 271 (2011) 523–528. doi:10.1016/j.wear.2010.03.029.
- [38] J. Eichstädt, G.R.B.E. Römer, A.J. Huis, Towards friction control using laser-induced periodic surface structures, *Phys. Procedia.* 12 (2011) 7–15. doi:10.1016/j.phpro.2011.03.099.
- [39] A. Ben-Yakar, R.L. Byer, A. Harkin, J. Ashmore, H.A. Stone, M. Shen, E. Mazur, Morphology of femtosecond-laser-ablated borosilicate glass surfaces, *Appl. Phys. Lett.* 83 (2003) 3030–3032. doi:10.1063/1.1619560.
- [40] A. Ben-Yakar, R.L. Byer, Femtosecond laser ablation properties of borosilicate glass, *J. Appl. Phys.* 96 (2004) 5316–5323. doi:10.1063/1.1787145.
- [41] A. Ben-Yakar, A. Harkin, J. Ashmore, R.L. Byer, H.A. Stone, Thermal and fluid processes of a thin melt zone during femtosecond laser ablation of glass: The formation of rims by single laser pulses, *J. Phys. D. Appl. Phys.* 40 (2007) 1447–1459. doi:10.1088/0022-3727/40/5/021.
- [42] K. Sugioka, Y. Cheng, Ultrafast lasers — reliable tools for advanced materials processing, *Light: Science & Applications* 3 (2014), e149:1-12. doi:10.1038/lssa.2014.30.
- [43] K. Sugioka, D. Wu, K. Midorikawa, Ship-in-a-bottle biomicrochips fabricated by hybrid femtosecond laser processing, *MATEC Web of Conferences*, 8 (2013) 05005:1-2.

- [44] S. Her, C. Huang, Effect of coating on the strain transfer of optical fiber sensors, *Sensors* 11 Sensors 11 (2011) 6926–6941. doi:10.3390/s110706926.
- [45] B. Li, L. Jiang, S. Wang, Q.C. Mengmeng Wang, J. Yang, A new Mach-Zehnder interferometer in a thinned-cladding fiber fabricated by electric arc for high sensitivity refractive index sensing, *Opt. Lasers Eng.* 50 (2012) 829–832. doi:10.1016/j.optlaseng.2012.01.024.
- [46] Z. Feng, J. Li, X. Qiao, L. Li, H. Yang, M. Hu, A thermally annealed Mach-Zehnder interferometer for high temperature measurement, *Sensors (Basel)*. 14 (2014) 14210–14221. doi:10.3390/s140814210.
- [47] M. Birnbaum, Semiconductor surface damage produced by Ruby lasers, *J. Appl. Phys.* 36 (1965) 3688–3689. doi:10.1063/1.1703071.
- [48] C. Teichert, Self-organization of nanostructures in semiconductor heteroepitaxy, *Phys. Rep.* 365 (2002) 335–432. doi:10.1016/S0370-1573(02)00009-1.
- [49] X. Wang, C.A. Ohlin, Q. Lu, J. Hu, Cell directional migration and oriented division on three-dimensional laser-induced periodic surface structures on polystyrene, *Biomaterials*. 29 (2008) 2049–2059. doi:10.1016/j.biomaterials.2007.12.047.
- [50] K. Oya, S. Aoki, K. Shimomura, N. Sugita, K. Suzuki, Morphological observations of mesenchymal stem cell adhesion to a nanoporous-structured titanium surface patterned using femtosecond laser processing, *Jpn. J. Appl. Phys.* 51 (2012) 125203. doi:10.1143/JJAP.51.125203.
- [51] B. Dusser, Z. Sagan, H. Soder, N. Faure, J.P. Colombier, M. Jourlin, E. Audouard, Controlled nanostructures formation by ultra fast laser pulses for color marking., *Opt. Express*. 18 (2010) 2913–2924. doi:10.1364/OE.18.002913.
- [52] B.-B. Xu, Z.-C. Ma, L. Wang, R. Zhang, L.-G. Niu, Z. Yang, Y.-L. Zhang, W.-H. Zheng, B. Zhao, Y. Xu, Q.-D. Chen, H. Xia, H.-B. Sun, Localized flexible integration of high-efficiency surface enhanced Raman scattering (SERS) monitors into microfluidic channels., *Lab Chip*. 11 (2011) 3347–3351. doi:10.1039/c1lc20397e.
- [53] J.E. Sipe, J.F. Young, J.S. Preston, H.M. Van Driel, Laser-induced periodic surface structure. I. Theory, *Phys. Rev. B.* 27 (1983) 1141–1154. doi:10.1103/PhysRevB.27.1141.
- [54] J.F. Young, J.S. Preston, H.M. Van Driel, J.E. Sipe, Laser-induced periodic surface structure. II. Experiments on Ge, Si, Al, and brass, *Phys. Rev. B.* 27 (1983) 1155–1172. doi:10.1103/PhysRevB.27.1155.
- [55] J.F. Young, J.E. Sipe, H.M. Van Driel, Laser-induced periodic surface structure. III. Fluence regimes, the role of feedback, and details of the induced topography in germanium material, *Phys. Rev. B.* 30 (1984) 2001–2015. doi:10.1103/PhysRevB.30.2001.

- [56] Q. Wu, Y. Ma, R. Fang, Y. Liao, Q. Yu, X. Chen, K. Wang, Femtosecond laser-induced periodic surface structure on diamond film, *Appl. Phys. Lett.* 82 (2003) 1703–1705. doi:10.1063/1.1561581.
- [57] A. Borowiec, H.K. Haugen, Subwavelength ripple formation on the surfaces of compound semiconductors irradiated with femtosecond laser pulses, *Appl. Phys. Lett.* 82 (2003) 4462–4464. doi:10.1063/1.1586457.
- [58] G. Miyaji, K. Miyazaki, Nanoscale ablation on patterned diamondlike carbon film with femtosecond laser pulses, *Appl. Phys. Lett.* 91 (2007) 2005–2008. doi:10.1063/1.2784966.
- [59] G. Miyaji, K. Miyazaki, Origin of periodicity in nanostructuring on thin film surfaces ablated with femtosecond laser pulses, *Opt. Express.* 16 (2008) 16265–16271. doi:10.1364/OE.16.016265.
- [60] M. Straub, M. Afshar, D. Feili, H. Seidel, K. König, Surface plasmon polariton model of high-spatial frequency laser-induced periodic surface structure generation in silicon, *J. Appl. Phys.* 111 (2012) 124315:1–6. doi:10.1063/1.4730381.
- [61] R. Le Harzic, D. Dörr, D. Sauer, M. Neumeier, M. Eppler, H. Zimmermann, F. Stracke, Large-area, uniform, high-spatial-frequency ripples generated on silicon using a nanojoule-femtosecond laser at high repetition rate, *Opt. Lett.* 36 (2011) 229–231. doi:10.1364/OL.36.000229.
- [62] M. Henyk, N. Vogel, D. Wolfframm, A. Tempel, J. Reif, Femtosecond laser ablation from dielectric materials: Comparison to arc discharge erosion, *Appl. Phys. A Mater. Sci. Process.* 69 (1999) 355–358. doi:10.1007/s003399900411.
- [63] J. Reif, F. Costache, M. Henyk, S. V Pandelov, Ripples revisited: Non-classical morphology at the bottom of femtosecond laser ablation craters in transparent dielectrics, *Appl. Surf. Sci.* (2002) 891–895. doi:10.1016/S0169-4332(02)00450-6.
- [64] F. Costache, S. Kouteva-arguirova, J. Reif, Sub – damage – threshold femtosecond laser ablation from crystalline Si<sup>⊙</sup>: Surface nanostructures and phase transformation, *Appl. Phys. A Mater. Sci. Process.* 1432 (2004) 1429–1432. doi:10.1007/s00339-004-2803-y.
- [65] J. Reif, O. Varlamova, F. Costache, Femtosecond laser induced nanostructure formation: Self-organization control parameters, *Appl. Phys. A Mater. Sci. Process.* 92 (2008) 1019–1024. doi:10.1007/s00339-008-4671-3.
- [66] J. Reif, F. Costache, O. Varlamova, G. Jia, M. Ratzke, Self-organized regular surface patterning by pulsed laser ablation, *Phys. Status Solidi Curr. Top. Solid State Phys.* 6 (2009) 681–686. doi:10.1002/pssc.200880719.
- [67] M. Huang, F. Zhao, Y. Cheng, N. Xu, Z. Xu, Origin of laser-induced near-subwavelength ripples: Interference between surface plasmons and incident laser, *ACS Nano.* 3 (2009) 4062–4070. doi:10.1021/nn900654v.

- [68] G.A. Martsinovskii, G.D. Shandybina, D.S. Smirnov, S. V Zaboltnov, L.A. Golovan, V.Y. Timoshenko, P.K. Kashkarov, Ultrashort excitations of surface polaritons and waveguide modes in semiconductors, *Opt. Spectrosc.* 105 (2008) 67–72. doi:10.1134/S0030400x08070114.
- [69] S. Sakabe, M. Hashida, S. Tokita, S. Namba, K. Okamuro, Mechanism for self-formation of periodic grating structures on a metal surface by a femtosecond laser pulse, *Phys. Rev. B – Condens. Matter Mater. Phys.* 79 (2009) 1–4. doi:10.1103/PhysRevB.79.033409.
- [70] K. Okamuro, M. Hashida, Y. Miyasaka, Y. Ikuta, S. Tokita, S. Sakabe, Laser fluence dependence of periodic grating structures formed on metal surfaces under femtosecond laser pulse irradiation, *Phys. Rev. B - Condens. Matter Mater. Phys.* 82 (2010) 1–5. doi:10.1103/PhysRevB.82.165417.
- [71] J. Bonse, M. Munz, H. Sturm, Structure formation on the surface of indium phosphide irradiated by femtosecond laser pulses, *J. Appl. Phys.* 97 (2005) 013538:1-9. doi:10.1063/1.1827919.
- [72] J. Bonse, A. Rosenfeld, J. Kruger, On the role of surface plasmon polaritons in the formation of laser-induced periodic surface structures upon irradiation of silicon by femtosecond-laser pulses, *J. Appl. Phys.* 106 (2009) 104910:1-5. doi:10.1063/1.3261734.
- [73] D. Dufft, A. Rosenfeld, S.K. Das, R. Grunwald, J. Bonse, Femtosecond laser-induced periodic surface structures revisited: A comparative study on ZnO, *J. Appl. Phys.* 105 (2009) 034908:1-9. doi:10.1063/1.3074106.
- [74] F. Baset, K. Popov, A. Villafranca, A.M. Alshehri, J.M. Guay, L. Ramunno, V.R. Bhardwaj, Nanopillar formation from two-shot femtosecond laser ablation of poly-methyl methacrylate, *Appl. Surf. Sci.* 357 (2015) 273–281. doi:10.1016/j.apsusc.2015.09.007.
- [75] E.G. Gamaly, A. V Rode, V.T. Tikhonchuk, E.G. Gamaly, A. V Rode, Ablation of solids by femtosecond lasers: Ablation mechanism and ablation thresholds for metals and dielectrics, *Phys. Plasmas.* 9 (2002) 949–957. doi:10.1063/1.1447555.
- [76] A. Borowiec, H.F. Tiedje, H.K. Haugen, Wavelength dependence of the single pulse femtosecond laser ablation threshold of indium phosphide in the 400–2050 nm range, *Appl. Surf. Sci.* 243 (2005) 129–137. doi:10.1016/j.apsusc.2004.09.105.
- [77] J. Noack, A. Vogel, Laser-induced plasma formation in water at nanosecond to femtosecond time scales: Calculation of thresholds, absorption coefficients, and energy density, *IEEE J. Quant. Electr.* 35 (1999) 1156-1167.
- [78] A. Kaiser, Microscopic processes in dielectrics under irradiation by subpicosecond laser pulses, *Phys. Rev. B* 61 (2000) 11437–11450.
- [79] H.M. Saulius, Juodkazis, Oleg A Louchev, Kenji Kitamura, Femtosecond laser ablation of chalcogenide glass: Explosive formation of nano-fibres against thermocapillary growth of micro-spheres, *Nanotechnology.* 17 (2006) 4. doi:10.1088/0957-4484/17/19/003.

- [80] K. Venkatakrishnan, D. Vipparthy, B. Tan, Nanofibre fabrication by femtosecond laser ablation of silica glass, *Opt. Express*. 19 (2011) 15770. doi:10.1364/OE.19.015770.
- [81] A. V. Rode, E.G. Gamaly, B. Luther-Davies, Formation of cluster-assembled carbon nano-foam by high-repetition-rate laser ablation, *Appl. Phys. A Mater. Sci. Process.* 70 (2000) 135–144. doi:10.1007/s003390050025.

IntechOpen

IntechOpen